Volume 19, No 4 | International Journal of Radiation Research, October 2021

Evaluation of the dosimetric characteristics of 10 MV flattened and unflattened photon beams in a heterogeneous phantom

S. Yani[1*], I. Budiansah[2], S.H. Pratama[2], M.F. Rhani[3], C. Anam[4], F. Haryanto[2]

[1]*Department of Physics, Faculty of Mathematics and Natural Sciences, IPB University, Bogor 16680, Indonesia*
[2]*Department of Physics, Faculty of Mathematics and Natural Sciences, Institut Teknologi Bandung, West Java, 40132, Indonesia*
[3]*Department of Radiology, Concord International Hospital, Singapore, 289891, Singapore*
[4]*Department of Physics, Faculty of Sciences and Mathematics, Diponegoro University, Central Java, Indonesia*

► ***Original article***

Corresponding author:
Sitti Yani Ph.D.,
E-mail:
sittiyani@apps.ipb.ac.id

Revised: December 2020
Accepted: January 2021
Int. J. Radiat. Res., October 2021; 19(4): 835-841
DOI: 10.29242/ijrr.19.4.835

ABSTRACT

Background: The free flattening filter (FFF) beam can affect the characteristics of the linac output such as the maximum dose depth, surface dose, dose in the fall-off area, and doses outside the field because the beam hardening effect does not occur in the FFF linac head. Therefore, the present study aimed to investigate the influence of the FFF beam on the dose distribution in an inhomogeneous phantom using the EGSnrc/DOSXYZnrc Monte Carlo package. ***Materials and Methods:*** In the present study, an Elekta Infinity 10 MV photon beam equipped with a multileaf collimator Agility linear accelerator was used. Two types of virtual inhomogeneous phantoms were built for percent depth doses (PDDs) and dose profiles measurement. The first phantom comprised four layers: water (4 cm thickness), bone (2 cm thickness), lung tissue (5 cm thickness), and water (19 cm thickness). The second phantom had a half-lung tissue slab and a half-bone slab (10 cm thickness) on the left side of the water. ***Results:*** The PDD curves in the inhomogeneous phantom considerably decreased in the lung area for small exposure fields because the charged particle equilibrium was not achieved. The dose in the lung was higher than the dose in the water when the charged particle equilibrium was reached. Meanwhile, the dose in the bone is always lower than the dose in the water. ***Conclusions:*** The dose distribution of flattening filter (FF) and FFF beams in the inhomogeneous phantom was the same in the small field of exposure. However, differences in dose distribution are increasingly apparent for larger field sizes.

Keywords: *Elekta Infinity, flattening filter free, EGSnrc, heterogeneous phantom.*

INTRODUCTION

In a conventional clinical linear accelerator (linac) with the energy range of 4–25 MV, the angular distribution of bremsstrahlung photons is predominantly in the direction of the incident electrons. These photons are further modified by a flattening filter (FF), which is placed in the beamline to homogenize the beam energy. Since the introduction of linac in the 1950s, FF has been regarded as an essential component. However, there are several unresolved issues regarding the use of FF. In modern clinical linear accelerators, including Varian and Elekta, these filters comprise conical-shaped pieces of metal and are typically made of high-Z materials, such as iron, copper, or tungsten, or their mixture; the metals used depend on the beam energy.

Several issues can occur because of the presence of an FF in linac. Specifically, the

[DOI: 10.52547/ijrr.19.4.9]

reduction of the dose rate can occur because of decreased primary beam intensity [1–4]; changes in beam spectrum cause problems for dose calculation and beam modeling [1,4–6]; a significant source of scattered radiation within the beam is created and produces particle contamination (electron and neutron) in the primary beam [7–10].

In recent years, research on flattening filter free (FFF) linac has experienced a significant increase in the number of publications, and many studies report the use of Monte Carlo (MC) simulations with various codes [1,6,7,11,12]. There are many publications on the dosimetric properties of FFF beams for Varian accelerators; however, presently, there are no publications on Elekta Infinity™ [13–15]. The comparison between photon beams produced with and without an FF in the beamline of an Elekta Precise linac using MC simulations has been also previously reported [12,15–17]. MC simulations and measurements have been combined by Daylard *et al.* (*2010*) to investigate the effect of the absence of an FF (a 6 mm copper plate was inserted in the treatment head) in an Elekta Precise linac [12]. This beam produced many head scatters. In an unflattened photon beam, Kragl *et al.* (*2009*) have placed the same plate in the beamline to compensate for the absence of an FF [15]. They determined that the average dose rate in the Elekta Precise unflattened beam was increased by two times compared with that of the flattened beam. Some treatment techniques (e.g., IMRT and VMAT) require a beam with a high dose rate; thus, this mode is very suitable. Tyler *et al.* (2016) have calculated the small field correction factor in unflattened mode Elekta Axesse. The clinical implementation of unflattened beam greatly affects the measured correction factor [16]. The relative dose in the Elekta Versa HD 6 and 10 MV unflattened beam was lower than that in the flattened beam because of an additional scattering caused by the presence of an FF [17].

The quantity of neutron contamination in the Elekta Infinity 10 MV unflattened beam was higher than that in the flattened beam; however, the beams had the same quality. We reported this result in our previous study. The effect of the absence of an FF in the treatment head in our previous study was limited, which allowed the investigation of the existence of particle contamination in the phantom surface [18]. The present study, which is an extension of the previous one, examines the effect of an unflattened beam on phantom's dosimetric characteristics.

The present study aimed to investigate the dosimetric effect after the removal of an FF from the Elekta Infinity™ 10 MV photon beam in a heterogeneous phantom. The use of this phantom is based on the fact that the human body comprises several types of materials.

MATERIALS AND METHODS

Modeling of a head linac

For the present study, an Elekta Infinity™ 10 MV photon beam was modified to enable irradiation delivery with and without the FF in the beamline. Linac head modeling is the initial stage in the particle transport simulation. For the MC modeling of the radiation transport through the linac head into the water, an EGSnrc -BEAMnrc/DOSXYZnrc package was used [19, 20]. The geometry and material of linac components were modeled based on the manufacturer data (Elekta Oncology Systems, Stockholm, Sweden). The linac components modeled in BEAMnrc were the target, primary collimator, difference filter, FF, back-scatter plate, ion chamber, mirror, and multileaf collimator (MLC). The geometry of each component was designed using component modules (CMs) that are available in the BEAMnrc user code. The CM used for each linac head component is listed in table 1. This linac head was commissioned to obtain an appropriate initial electron energy and full width at half maximum in the simulation.

The MC model for this linac simulation was operated with the presence (FF mode) and the absence (FFF mode) of the FF. The simulations were conducted for the square field sizes of 1 × 1, 2 × 2, 3 × 3, 4 × 4, 10 × 10, 15 × 15, and 20 × 20 cm^2.

[DOI: 10.52547/ijrr.19.4.9]

Table 1. Component modules (CMs) used for modeling the head linac components.

No.	Head linac components	CMs
1	Target	SLABS
2	Primary collimator and difference filter	FLATFILT
3	Flattening filter	FLATFILT
4	Ion chamber	CHAMBER
5	Back-scatter plate	SLABS
6	Mirror	MIRROR
7	MLC	MLCE
8	Air (defined between the MLC and phantom)	SLABS

Phantom design

Virtual phantom design and dose calculations were conducted using the DOSXYZnrc user code. The heterogeneous water phantom of 40 × 40 × 40 cm^3, which was recommended by the manufacturer, was placed at the source to surface distance = 100 cm and contained water, bone, lung, and air. The phantom is modeled to comprise several volume elements (voxels) to facilitate the analysis of dose distribution. The phantom design for the percent depth dose (PDD), dose profile, and gamma index calculation was different, which made the simulation time more efficient.

The virtual heterogeneous phantom for the PDD calculation that was built is shown in figure 1. The heterogeneous model comprised four layers: water (4 cm thickness), bone (2 cm thickness), lung tissue (5 cm thickness), and water (29 cm thickness) (figure 1). This phantom was adopted from Onizuka *et al.* (2016) [21]. The voxel on the surface, build-up, and tail region of the phantom were differentiated to make the simulation efficient.

Two phantoms were used to analyze the profile dose in the heterogeneous medium. The first phantom comprised bone and water media, and the second phantom design comprised lung and water media (figure 2). The phantom design with a different medium is used to analyze the dose profile if it enters different types of media. Furthermore, this phantom design adopted that used in the Onizuka *et al.* (2016) study [21].

The phantom design for gamma index calculations is made with a size of 40 × 40 × 40 cm^3. The phantom was divided into 80 voxels for x, y, and z directions with a 0.5 cm voxel size.

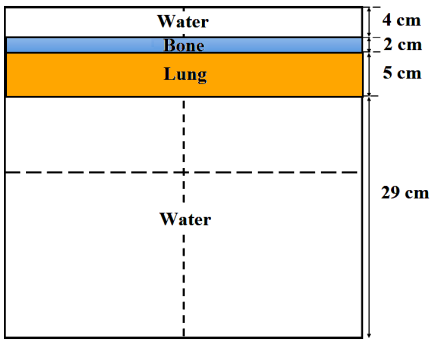

Figure 1. Phantom heterogeneous design for PDD calculation.

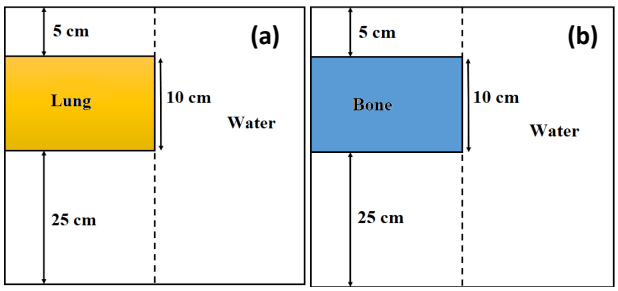

Figure 2. Heterogeneous phantom design for dose profile calculation: **(a)** bone and water medium and **(b)** lung and water medium.

Simulation parameters in DOSXYZnrc

The source used in this step is the phsp file obtained from the BEAMnrc simulation of the phantom's surface. Therefore, isource 2: phase–space source incident from any direction was selected. The defined parameters are shown in table 2. The phsp file contains particle information produced by linac's simulation, which includes the type of particle charge, energy, position, and weight.

The photon and electron cut-off energies were set to 10 keV (PCUT) and 711 keV (ECUT). No variance reduction techniques were applied in this simulation. Other EGSnrc parameters were set as default. The number of particles simulated was 1.2 × 10^9 histories. 3ddose files were produced at the end of the simulation containing the coordinate of voxels in x, y, and z directions, dose distribution in each voxel, and dose error. The dose error value was related to the statistical uncertainty of simulation.

In the present study, statistical uncertainty was not calculated manually, but it was one of

[DOI: 10.52547/ijrr.19.4.9]

the simulation outputs. A standard batching method was used. This statistical uncertainty depends on the number of histories simulated to reduce the simulation variance. The number of particles is inversely proportional to the variance and efficiency of the simulation [20, 22].

Table 2. Parameters defined in the isource 2 in DOSXYZnrc [17].

Parameters in DOSXYZnrc	Description	Value
xiso, yiso, ziso	x, y, and z coordinates of the isocenter	0, 0, and 20
Theta	Angle between the +z direction and a line joining the origin in the phase–space plane to the isocenter (in degrees)	180
Phi	Angle between the +x direction and the projection of the line joining the origin in the phase–space plane to the isocenter on the xy plane (in degrees)	0
Phicol	Angle by which the collimator is rotated in the collimator plane perpendicular to the beam direction (in degree)	0
dsource	Absolute distance from the origin of the phsp file to the coordinate of the isocenter (in cm)	20

RESULTS

The statistical uncertainty of this simulation was less than 1% for all cases. The dose rate in the present study indicated that the FFF beam was higher than the FF because there was no beam hardening, which increased the beam quantity in FFF (table 2).

PDDs

The beam hardening effect was also observed in PDDs (figure 3). The surface dose in FF was higher than that in FFF but was in reverse with the fall-off region. d_{max} at the field size of 2 × 2 cm^2 shifts 0.2 cm into a shallower depth for the linac head with the FF and FFF of 2.1 and 1.9 cm, respectively. However, these 0.2 cm shifts can still be considered based on the 3%/3 mm acceptance criterion.

Dose profiles

The dose profiles in the heterogeneous medium at the depth of 10 cm from the phantom surface are shown in figure 4. Doses in the lungs are always higher than those in the water for large field sizes, whereas in small field sizes, doses in the lungs are smaller than those in the water. The effect of FF presence can be observed from the flat form of the dose profile in each medium. The curvature pattern of FFF dose profiles was also observed in each medium for large field sizes. The dose reduction in FF and FFF in each medium for all field sizes is shown in table 4.

Gamma passing rate

The gamma index's value in a heterogeneous phantom for the field size of 10 × 10 cm^2 of FF and FFF beams at various depths is shown in figure 5. As shown in this figure, in the broad field size, the dose distribution can be considered the same only for the area around the beam axis. This pattern can also be seen in the dose profile, which coincides only in the area around the central axis. Meanwhile, in areas far from the beam axis, there was a massive difference in dose distribution because the FFF's dose profile curve is increasingly apparent. Meanwhile, the gamma passing rate values for some field sizes are shown in table 5.

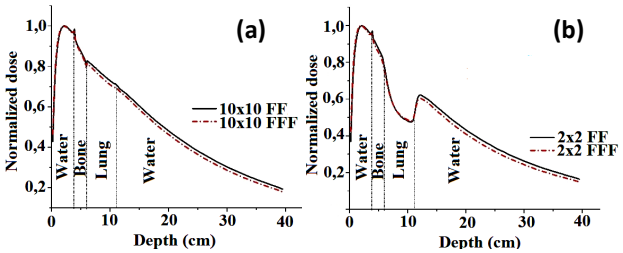

Figure 3. PDD for 10 MV photon beam for FF and FFF in a heterogeneous phantom for field sizes of **(a)** 10 × 10 cm^2 and **(b)** 2 × 2 cm^2.

Table 3. Comparison of the dose rate of FFF and FF for a small field size.

Field size (cm^2)	Dose rate of FFF / Dose rate of FF
1 × 1	2.10
2 × 2	2.09
3 × 3	2.08
4 × 4	2.07

[DOI: 10.52547/ijrr.19.4.9]

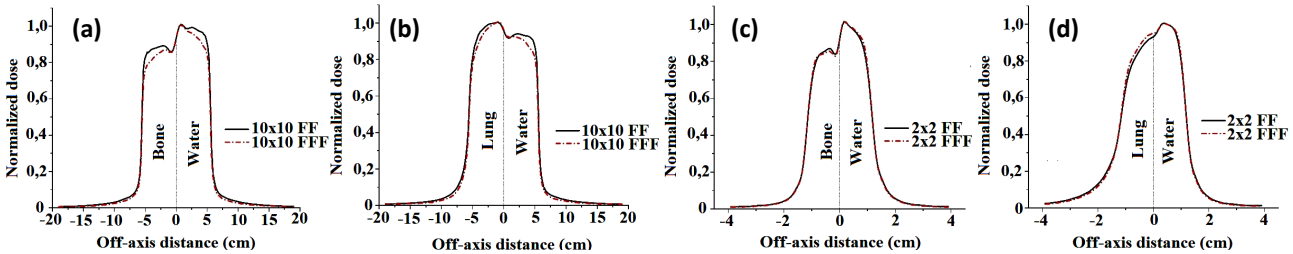

Figure 4. Dose profiles in a heterogeneous phantom for d = 10 cm and SSD = 100 cm **(a)** at 10 × 10 cm^2 for bone and water medium, **(b)** at 10 × 10 cm^2 for lung and water medium, **(c)** at 2 × 2 cm^2 for bone and water medium, and **(d)** at 2 × 2 cm^2 for lung and water medium.

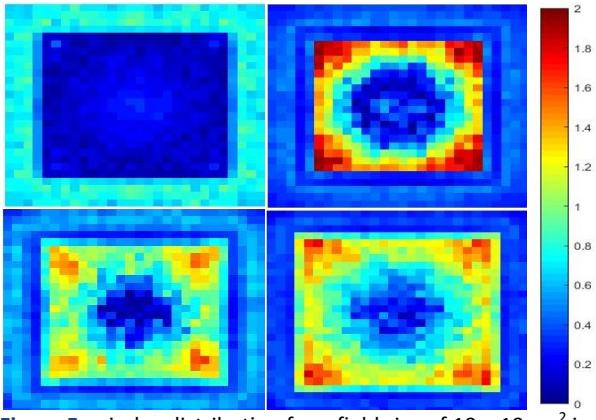

Figure 5. γ-index distribution for a field size of 10 × 10 cm^2 in a heterogeneous phantom for the following depths: **(a)** d = 0.25 cm (water), **(b)** d = 5.25 cm (bone), **(c)** d = 10.25 cm (lung), and **(d)** d = 20.25 cm (water).

Table 4. Comparison of dose reduction at the interface of FFF and FF outside the field size at a 10 cm depth.

Field size (cm^2)	Dose reduction in lung and water medium (%)		Dose reduction in bone and water medium (%)	
	Lung	Water	Bone	Water
1 × 1	1.93	5.56	4.36	3.56
2 × 2	4.28	5.82	2.68	3.23
3 × 3	3.70	5.05	3.57	4.84
4 × 4	7.34	6.07	2.48	4.44
10 × 10	14.86	15.15	13.77	15.24
15 × 15	18.86	17.48	17.04	19.69
20 × 20	25.45	25.78	25.54	28.91

Table 5. Gamma passing rates (GPR) for all field sizes.

Field sizes (cm^2)	GPR for all phantoms (%)	GPR in the area around the central beam axis (%)
1 × 1	100	100
2 × 2	100	100
3 × 3	100	100
4 × 4	100	100
10 × 10	97.87	82.58
15 × 15	87.24	61.40
20 × 20	70.78	36.03

DISCUSSION

The dose rate results shown in table 3 agree with the results obtained by Sangeetha and Sureka (2017) and Mahdavi *et al.* (2019) who reported that the dose rate around the beam axis of FFF was approximately two times higher for all field sizes [4, 23]. The beam hardening in FF can reduce surface doses; however, FF contributes to the generation of secondary radiation sources (neutron and electron contamination), which causes particles to scatter at large angles on the phantom surface.

PDDs in the heterogeneous phantom are shown in figure 4. As shown in this figure, there was an upstream pattern before entering the bone and a downstream pattern when it exited the bone. The same results have been reported by Reynaert *et al.* (2018), who investigated PDDs in water and bone media [24]. The bone density (1.85 g/cm^3) was higher than those of the water (1 g/cm^3) and lung (0.26 g/cm^3), which produced many low-energy back-scatter electrons at the border between the water and bone, which increases the dose in the water in that area and results in an upstream pattern [21].

[DOI: 10.52547/ijrr.19.4.9]

The dose in the lung medium considerably decreased in a small field because the lateral equilibrium of charged particles was not reached. In a small field, electrons produced by a 10 MV photon beam in the lung medium have better range than the size of defined voxels. This makes many electrons to deposit the dose outside the exposure field, which considerably decreases the dose in the lung medium. With an increase in field sizes, the pattern of dose reduction in the lungs is no longer observed because the lateral equilibrium of charged particles has been reached.

The dose profiles are shown in figure 4. The lungs have a lower density than the water, which causes reduced beam attenuation and results in the reduced scattering of the lungs. Therefore, the particles in the lung deposit are higher because of fewer scattered particles. In large field sizes, the lateral equilibrium of charged particles is reached because the range of secondary electrons is smaller than the field size. Consequently, the dose in the lungs is higher than that in the water. This phenomenon contrasts with what occurs at the interface the water and bones. This study was in line with the study conducted by Onizuka *et al.* (2016) [21].

The gamma passing rate for a field size of 10 × 10 cm^2 was unaffected by the FF in the central beam axis. Georg *et al.* (2011) performed an analysis of the difference in gamma index between FF and FFF on 10 MV Elekta Precise linac. They found the same result with this present study which found almost the same distribution of gamma values between these two beams for 10 × 10 cm^2 field [25]. Meanwhile, the dose distribution in small field sizes can be considered the same between the beam from the head of the linac with FF and FFF even in the central beam (table 5). This is because the beam's characteristics in the small field are the same because of the relatively small MLC openings.

CONCLUSIONS

The absence of an FF in a linac caused changes in heterogeneous phantom in the PDDs, dose profiles, and gamma passing rate, especially for a large field size (≥10 × 10 cm^2). The dose on the phantom surface on the FFF is higher than that on the FF because of electron contamination. The PDD curve in the heterogeneous phantom decreases dramatically in the lung area for the small field because of the inability to achieve charged particle equilibrium.

***Conflicts of interest*:** *Declared none.*

REFERENCES

1. Vassiliev ON, Titt U, Pönisch F, Kry SF, Mohan R, Gillin MT (2006) Dosimetric properties of photon beams from a flattening filter free clinical accelerator. *Physics in Medicine and Biology, **51(7)**: 1907-1917*.
2. Ceberg C, Johnsson S, Lind M, Knöös T (2010) Prediction of stopping-power ratios in flattening-filter free beams. *Medical Physics, **37(3)**: 1164-1168*.
3. Zavgorodni S (2013) Monte Carlo investigation into feasibility and dosimetry of flat flattening filter free beams. *Physics in Medicine and Biology, **58(21)**: 7699-7713*.
4. Sangeetha S and Sureka CS (2017) Comparison of Flattening Filter (FF) and Flattening-Filter-Free (FFF) 6MV photon beam characteristics for small field dosimetry using EGSnrc Monte Carlo code. *Radiation Physics and Chemistry, **135**: 63-75.*
5. Cashmore J (2008) The characterization of unflattened photon beams from a 6 MV linear accelerator. *Physics in Medicine and Biology, **53(7)**: 1933-1946*.
6. Mohammed M, Chakir E, Boukhal H, Mroan S,El Bardouni T (2017) Evaluation of the dosimetric characteristics of 6MV flattened and unflattened photon beam. *Journal of King Saud University – Science, **29(3)**: 371-379*.
7. Pönisch F, Titt U, Vassiliev ON, Mohan R (2006) Properties of unflattened photon beams shaped by a multileaf collimator: unflattened photon beam shaped by MLC. *Medical Physics, **33**: 1738–1746*.
8. Yani S, Dirgayussa IGE, Rhani MF, Soh RCX, Haryanto F, Arif I 2016 Monte Carlo study on electron contamination and output factors of small field dosimetry in 6 MV photon beam. *Smart Science, **4(2)**: 87-94*.
9. Yani S, Tursinah R, Rhani MF, Soh RCX, Haryanto F, Arif I (2016) Neutron contamination of varian clinac iX 10 MV photon beam using Monte Carlo simulation. *Journal of Physics: Conference Series, **694**: 012020.*
10. Yani S, Rhani MF, Soh RCX, Haryanto F, Arif I (2017) Monte Carlo simulation of Varian clinac iX 10 MV photon beam for small field dosimetry. *Int J Radiat Res, **15(3)**: 275-282*.
11. Titt U, Vassiliev ON, Pönisch F, Dong L, Liu H, Mohan R (2006) A flattening filter free photon treatment concept evaluation with Monte Carlo. *Medical Physics, **33(6)**: 1595*

[DOI: 10.52547/ijrr.19.4.9]

-1602.
12. Dalaryd M, Kragl G, Ceberg C, Georg D, McClean B, af Wetterstedt S, Wieslander E, Knöös T (2010) A Monte Carlo study of a flattening filter-free linear accelerator verified with measurements. *Physics in Medicine and Biology,* ***55(23)****: 7333-7344*.
13. Fu W, Dai J, Hu Y, Han D, Song Y (2004) Dosimetric properties of photon beams from a flattening filter free clinical accelerator. *Physics in Medicine and Biology,* ***49(8)****: 1535-1547*.
14. Zhu X R, Kang Y, Gillin MT (2006) Measurements of in-air output ratios for a linear accelerator with and without the flattening filter *Medical Physics,* ***33(10)****: 3723-3733*.
15. Kragl G, af Wetterstedt S, Knäusl B, Lind M, McCavana P, Knöös T, McClean B, Georg D (2009) Dosimetric characteristics of 6 and 10MV unflattened photon beams. *Radiotherapy and Oncology,* ***93(1)****: 141-146*.
16. Baic B, Kozłowska B, Kwiatkowski R, Dybek M (2019) Clinical advantages of using unfl attened 6-MV and 10-MV photon beams generated by the medical accelerator Elekta Versa HD based on their dosimetric parameters in comparison to conventional beams. *Nukleonika*, ***64(3)****: 77-86*.
17. Tyler MK, Liu PZY, Lee C, McKenzie DR, Suchowerska N (2016) Small field detector correction factors: effects of the flattening filter for Elekta and Varian linear accelerators. *Journal of Applied Clinical Medical Physics,* ***17(3)****: 223-235*.
18. Yani S, Budiansah I, Lestari FP, Tursinah R, Rhani MF, Haryanto F (2020) Investigation of neutron contamination of flattening filter and flattening filter-free 10-MV photon beams in Elekta Infinity™ accelerator. *Iranian Journal of Medical Physics,* ***17****: 126-132*.
19. Rogers DWO, Walters B, Kawrakow I (2018) BEAMnrc Users Manual (Ottawa: National Research Council of Canada)
20. Walters B, Kawrakow I, Rogers DWO (2018) DOSXYZnrc user's manual (Ottawa: National Research Council of Canada).
21. Onizuka R, Araki F, Ohno T, Nakaguchi Y, Kai Y, Tomiyama Y, Hioki K (2016) Accuracy of dose calculation algorithms for virtual heterogeneous phantoms and intensity-modulated radiation therapy in the head and neck. *Radiological Physics and Technology,* ***9:*** *77–87*.
22. Walters B, Kawrakow I, Rogers DWO (2002) History by history statistical estimators in the BEAM code system. *Medical Physics*, ***29:*** *2745–2752*.
23. Mahdavi R, Ay MR, Zabihzadeh M, Allahverdi M, Shahriari M, Hoseini-Ghahfarokhi M (2019) A full quantitative analysis of 18 MV photon beam from 2100 C/D-Varian clinical linear accelerator with and without flattening filter. *Int J Radiat Res,* ***17(1)****: 137-146*.
24. Reynaert N, Crop F, Sterpin E, Kawrakow I, Palmans H (2018) On the conversion of dose to bone to dose to water in radiotherapy treatment planning systems. *Physics and Imaging in Radiation Oncology*, ***5****: 26–30*.
25. Georg D, Knöös T, McClean B (2011) Current status and future perspective of flattening filter free photon beams. *Medical Physics,* ***38(3):*** *1280-1293.*

[DOI: 10.52547/ijrr.19.4.9]